ARTICLE

Periostin secreted by cancer-associated fibroblasts promotes cancer stemness in head and neck cancer by activating protein tyrosine kinase 7

Binbin Yu[1,2], Kailiu Wu[1], Xu Wang[1,2], Jianjun Zhang[1,2], Lizhen Wang[3], Yingying Jiang[1,2], Xuedan Zhu[1], Wantao Chen[1,2] and Ming Yan[1,2]

Abstract

Protein tyrosine kinase 7 (PTK7) and cancer-associated fibroblasts (CAFs) play important roles in cancer stemness, respectively. However, little is known about interaction between CAFs and PTK7 in cancers. In this study, we showed that PTK7 was significantly correlated with the Wnt/β-Catenin pathway and aggressive clinicopathologic features in human head and neck squamous cell carcinoma (HNSCC). Meanwhile, animal experiments showed that PTK7 enhanced chemoresistance and lung metastasis of HNSCC in vivo. In addition, co-immunoprecipitation (co-IP) assay demonstrated that POSTN secreted by CAFs was a potential upstream ligand of PTK7 which might act as a receptor. Further analysis revealed that POSTN promoted the cancer stem cell (CSC)-like phenotype via PTK7–Wnt/β-Catenin signaling, including the proliferation and invasion of HNSCC cells in vitro, as well as tumor initiation and progression in vivo. Collectively, our study proved that CAF-derived POSTN might promote cancer stemness via interacting with PTK7 in HNSCC, suggesting that the combination of POSTN and PTK7 might be a potential prognostic and diagnostic indicator and a promising therapeutic target.

Introduction

The mechanisms of carcinogenesis and development of head and neck cancer (HNC), the seventh most common cancer worldwide, are poorly understood[1]. Elective neck dissection has remarkedly improved the overall survival (OS) rates of patients with early-stage disease, but many patients are actually overtreated[2]. Therefore, there is still an urgent need to determine the cellular and molecular mechanisms of HNCs.

Among tumor cells, there are small fractions of cells known as cancer stem cells (CSCs), which are related to proliferation, differentiation ability, metastasis, and chemotherapy resistance[3–6]. Our previous study demonstrated that protein tyrosine kinase 7 (PTK7) is highly expressed in head and neck squamous cell carcinoma (HNSCC) sphere-forming cells compared to adherent cells[7], which suggests that PTK7 acts as a CSC marker in HNSCC. PTK7 is also reported to be a surface marker for the isolation of human colon stem cells, which have higher self-renewal and reseeding capacity[8]. Also known as colon carcinoma kinase-4 (CCK-4), PTK7 is known to be upregulated in various types of cancer, including gastric cancer, colon cancer, esophageal cancer, and breast cancer, and is associated with drug resistance, elevated

Correspondence: Wantao Chen (chenwantao196323@sjtu.edu.cn) or Ming. Yan (yanming8012@126.com)
[1]Department of Oral and Maxillofacial-Head & Neck Oncology, Shanghai Ninth People's Hospital & College of Stomatology, Shanghai Jiao Tong University School of Medicine, Shanghai 200011, China
[2]National Clinical Research Center of Stomatology, Shanghai Key Laboratory of Stomatology & Shanghai Research Institute of Stomatology, Shanghai 200011, China
Full list of author information is available at the end of the article.
These authors contribute equally: Binbin Yu, Kailiu Wu
Edited by A. Stephanou

metastatic ability, and poor survival[9,10]. Furthermore, PTK7 is reported to be associated with the Wnt pathway[11–15], which is related to the regulation of CSCs[4,16,17]. Wnt signaling is activated through the canonical Wnt/β-Catenin pathway, the Wnt/Ca^{2+} pathway, and the planar cell polarity pathway[18]. The initiation and progression of cancer are mostly related to the canonical pathway[10,18]. However, whether PTK7 acts as a promoter or inhibitor of the canonical Wnt/β-Catenin pathway is still controversial[13–15].

Periostin (encoded by *Postn*) is a matricellular protein secreted by cancer-associated fibroblasts (CAFs), which may promote cancer stemness, initiation, and progression[19,20], and is overexpressed in many cancers, such as breast cancer, colon cancer, glioblastoma, gastric cancer, and liver cancer[21–25]. Many reports have demonstrated that POSTN promoted the CSC-like phenotype of tumor cells and was related to the canonical Wnt/β-Catenin pathway[25–28]. Our previous study demonstrated that POSTN was highly expressed in tumor stroma compared to tumor cells and that it promoted tumor progression and metastasis in HNSCC[29]. However, whether POSTN maintains the CSC-like phenotype in HNSCC via PTK7–Wnt signaling is still unknown. Given that POSTN and PTK7 are both related with the Wnt/β-Catenin pathway, we assume that there exists some molecular link between POSTN and PTK7.

To determine the molecular link among POSTN, PTK7, and the canonical Wnt/β-Catenin pathway in HNSCC, we first analyzed the expression patterns of PTK7 and its correlation with clinicopathologic significance. The relationship between PTK7 and β-Catenin/Wnt signaling was also analyzed. Moreover, we investigated the molecules secreted by CAFs with which PTK7 interacts and focused on POSTN. The effects of POSTN and PTK7 on cancer stemness and the proliferation and invasion of tumor cells were measured both in vitro and in vivo. The potential relationship among PTK7, POSTN, and the canonical Wnt/β-Catenin pathway was clarified. In this study, we found that the POSTN-PTK7 axis plays an important role in the CSC-like phenotype and the tumor progression and metastasis of HNSCC, suggesting that it is a potential prognostic marker and therapy target of HNSCCs.

Results
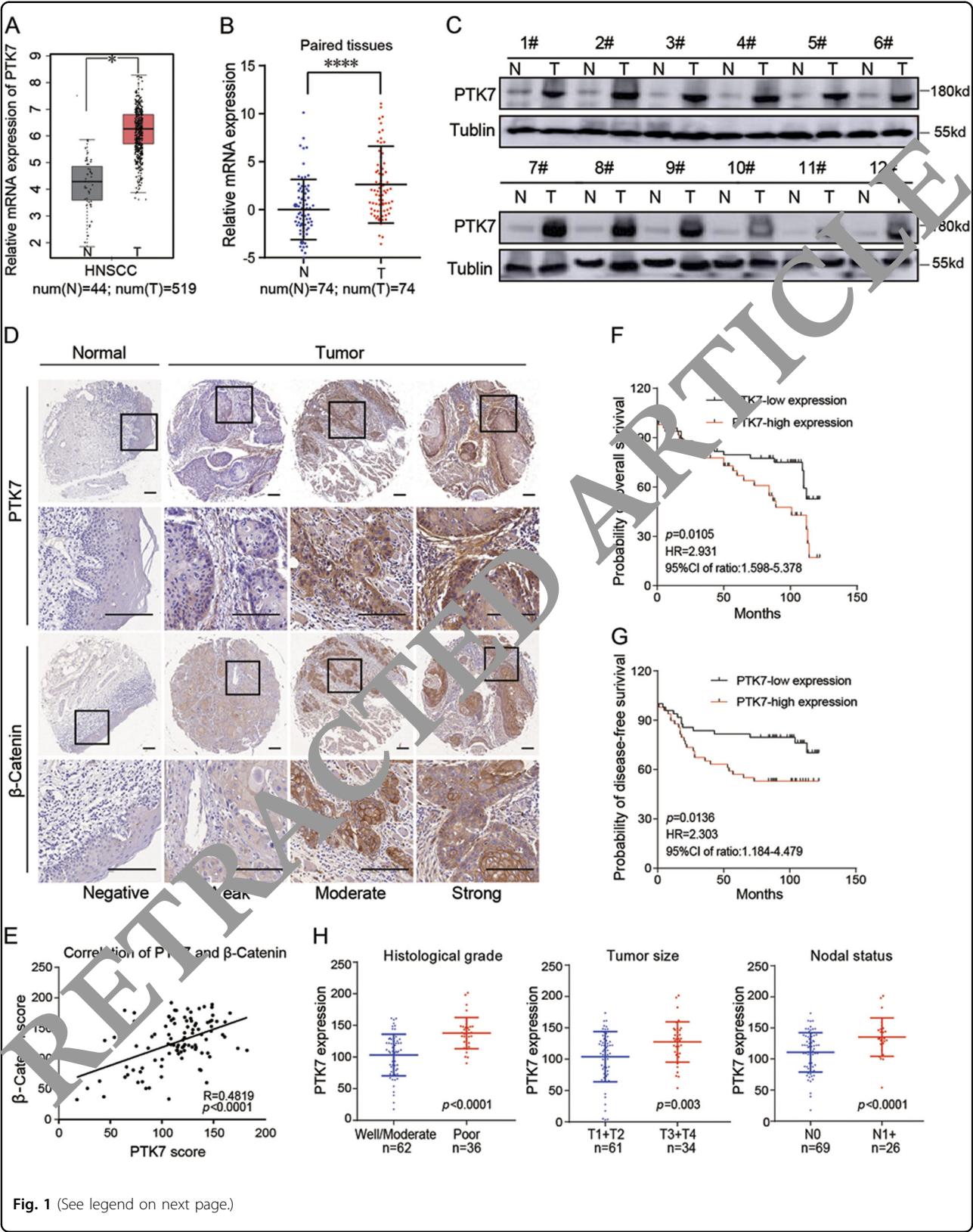### Increased PTK7 expression is correlated with the Wnt/β-Catenin pathway and increased aggressive clinicopathologic features in HNSCC

Analysis of the Cancer Genome Atlas (TCGA) dataset showed that PTK7 is highly expressed in many tumors (Supplementary Figure 1A), and higher PTK7 levels are correlated with poor disease-free survival (DFS) in human HNSCC (Supplementary Figure 1B). The PTK7 gene was expressed at high levels in HNSCC tissues compared to

normal tissues (Fig. 1a). The results of reverse transcriptase polymerase chain reaction (RT-PCR) indicated that PTK7 mRNA levels were higher in tumor tissues than in adjacent normal tissues (Fig. 1b). Correspondingly, western blot showed that the protein levels of PTK7 were also significantly upregulated in HNSCC tissues compared to normal tissues (Fig. 1c). Since PTK7 acts as a regulatory factor of the canonical Wnt/β-Catenin pathway, we analyzed the correlation between PTK7 and β-Catenin expression by immunohistochemistry (IHC), whose results showed that normal tissues and HNSCC tissues displayed concordant negative, weak, moderate, and strong PTK7 and β-Catenin staining (Fig. 1d). The data showed that β-Catenin expression was positively correlated with PTK7 expression ($R = 0.4819$, $p < 0.0001$) (Fig. 1e), which was consistent with the data in TCGA (Supplementary Figure 1C). We then analyzed the clinical significance of the changes in PTK7 expression in HNSCC. As shown in Table 1 and Fig. 1h, high PTK7 expression levels were associated with a poor histological grade, a large tumor size (greater than 4 cm in diameter), and nodal metastasis in the HNSCC specimens; however, PTK7 expression levels were not associated with the following parameters: age, gender, smoking, alcohol, and local recurrence. Kaplan–Meier analysis was performed to analyze the OS and the DFS of HNSCC patients. The results showed that the HNSCC patients with strong PTK7 staining had poorer OS ($p = 0.01051$) (Fig. 1f) and poorer DFS ($p = 0.0136$) (Fig. 1g). Cox regression analyses revealed that PTK7 expression was significantly correlated with poor OS in the patients with HNSCC and was an independent predictor of prognosis in such patients (Table 2). Taken together, these data indicate that PTK7 expression is frequently upregulated in human HNSCC tissues and is correlated with the Wnt/β-Catenin pathway and poor clinical outcomes in HNSCC patients.

Inhibition of PTK7 enhanced erlotinib efficacy and reduced β-Catenin expression and mouse lung metastasis in vivo

Many studies have reported that CSCs contributed to chemoresistance[5,30]. Erlotinib is a small-molecule tyrosine kinase inhibitor that inhibits the kinase domain of the EGFR[31] and has been tested in the clinic as treatments for recurrent and/or metastatic HNSCC[32–34]. We determined to test whether PTK7 inhibition reduced tumor progression and increased erlotinib sensitivity in vivo. As shown in Fig. 2a, b, tumor volume and weight in each treatment group were significantly decreased compared to those in the control group. Additionally, tumor volume and weight in the group treated with the combination of the PTK7 antibody and erlotinib were significantly lower than those in the groups treated with the PTK7 antibody or erlotinib alone (Figs. 2a, b, Supplementary Figure 1D and 1E). There was no morphological difference in hematoxylin

Fig. 1 (See legend on next page.)

(see figure on previous page)

Fig. 1 Increased PTK7 expression is correlated with the Wnt/β-Catenin pathway and aggressive clinicopathologic features and predicts a poor prognosis in HNSCC. a Relative PTK7 mRNA expression levels in normal tissues and HNSCC tissues from TCGA database are shown. *$p < 0.05$. **b** Relative PTK7 mRNA levels in 74 paired adjacent normal tissues and HNSCC tissues were evaluated by RT-PCR. ****$p < 0.0001$, based on the paired *t*-test. **c** PTK7 protein expression levels in 12 paired adjacent normal tissues and HNSCC tissues were determined by western blot. Tubulin was used as a loading control. **d** IHC analysis of PTK7 and β-Catenin expression levels in tissue microarrays containing 10 normal tissues and 98 HNSCC tissues. Images of negative, weak, moderate, and strong PTK7 and β-Catenin staining are shown. Scale bar: 20 μm. **e** The correlation of PTK7 and β-Catenin expression was analyzed in tissue microarrays containing 10 normal tissues and 98 HNSCC tissues ($R = 0.4819$, $p < 0.001$). **f** OS was significantly different between the low and high PTK7 expression groups in HNSCC ($p = 0.0105$, HR = 2.931, 95% CI of ratio: 1.598–5.378). **g** DFS was significantly different between the low and high PTK7 expression groups in HNSCC ($p = 0.0136$, HR = 2.303, 95% CI of ratio: 1.184–4.479). **h** PTK7 protein expression levels were significantly associated with historical grade, tumor size, and nodal status

and eosin (H&E) staining in the tumors among the four groups (Fig. 2c). IHC analysis of Ki67, PTK7, and β-Catenin expression demonstrated that the numbers of Ki67-, PTK7-, and β-Catenin- positive cells in the three treatment groups were significantly lower than those in the control group and that the combined treatment group showed a significantly greater decrease than the groups treated with the PTK7 antibody or erlotinib alone (Fig. 2d).

To investigate the role of PTK7 in lung metastasis models, the lungs were isolated at 0, 1, and 4 days and at 1 and 2 weeks (Supplementary Figure 1F). Whole-mount pictures revealed that tumor cell numbers decreased during the first week; in week 2, the tumor colonies took up virtually the entire lung (Supplementary Figure 1G). The PTK7 antibody group had fewer tumor cells and colonies than the control group ($p < 0.001$) (Supplementary Figure 1G). Consistent with these results, H&E staining and the lung weight data revealed that the PTK7 antibody decreased colony numbers and lung weight compared to the control treatment ($p < 0.001$) (Figs. 2e, f and Supplementary Figure 1H). Taken together, these data suggest that PTK7 inhibition enhanced erlotinib efficacy and reduced β-Catenin expression and lung metastases in vivo.

POSTN secreted by CAFs is a potential ligand of PTK7

The immunohistochemical analysis of PTK7 expression in HNSCC tissues revealed that PTK7 was mainly upregulated in the tumor cells and was weakly expressed in the tumor stroma (Supplementary Figure 2A). To detect the distribution of PTK7 in HNSCC tissues, we isolated normal fibroblasts (NFs) and CAFs from adjacent normal tissues and tumor tissues of HNSCC patients. Western blot showed that PTK7 was highly expressed in the tumor cells compared to the stromal cells and that PTK7 expression levels in the CAFs were higher than those in the NFs (Supplementary Figure 2B). To evaluate the purity of CAFs, western blot showed that the expression of E-cadherin (a protein mainly expressed on the cell surface of most epithelial tissues) was high in tumor cells

but almost none in CAFs. Similarly, the expression of Vimentin (a protein mainly expressed in mesenchymal cells) was high in CAFs, but relatively lower in tumor cells (Supplementary Figure 2C). PTK7 protein levels in the HNSCC cell lines were increased compared to those in the normal oral epithelial cells and NFs (Supplementary Figure 2C and D). Interestingly, IHC showed that there was strong PTK7 staining at the boundary between the tumor cells and tumor stroma (Supplementary Figure 2A), suggesting that PTK7 played a role in the interaction between the tumor cells and stromal cells. To further investigate the interaction between PTK7 and CAFs, we performed co-immunoprecipitation (co-IP) assay. The gel was silver stained (Fig. 3a) and performed mass spectrometry (MS) analysis. Several proteins secreted by CAFs, including POSTN, Dermcidin (DCD), and a 78-kDa glucose-regulated protein (HSPA5), were identified from the immunoprecipitated elution (Fig. 3b, Supplementary Figure 3A and B, Supplementary Tables 1 and 2). According to TCGA dataset, POSTN was most significantly correlated with PTK7 (Pearson R value = 0.59) (Supplementary Figure 3C). We then analyzed the correlation between POSTN and PTK7 in other types of tumors, including Bladder Urothelial Carcinoma (BLCA), Cholangiocarcinoma (CHOL), Kidney Chromophobe (KICH), Pancreatic adenocarcinoma (PAAD), and the results showed that POSTN was most highly correlated with PTK7 in the tumors (Supplementary Figure 3D–3F). In addition, POSTN staining revealed that POSTN was mainly located in the tumor stroma (Supplementary Figure 2E). Western blot demonstrated that POSTN was mainly expressed in CAFs rather than in NFs and tumor cells (Supplementary Figure 2F), a finding consistent with those of our previous study.

As shown in Supplementary Figure 2D, PTK7 expression levels were higher in the SCC-25 and HN6 cell lines but were lower in the CAL 27 cell line. We performed co-IP assay in the co-cultured system of HN6 + CAFs and SCC-25 + CAFs and the results revealed an endogenous interaction between POSTN and PTK7 (Figs. 3c, d). In addition, the immunofluorescence imaging revealed the

Table 1 Demographic characteristics of the patient population according to PTK7 expression

	PTK7		p-Value
	<121.4275	>121.4275	
All cases	49	49	
Age, years			0.838
<60 y	28	29	
≥60 y	21	20	
Gender			
Male	26	26	0.580
Female	23	23	
Smoking history			
Yes	24	9	0.807
No	25	40	
Alcohol history			
Yes	21	18	0.748
No	28	31	
Histological grade (differentiation)			**0.000**
Well/moderate	41	21	
Poor	8	28	
Tumor size			**0.003**
T1 + T2	38	23	
T3 + T4	9	25	
Unknown	2	1	
Nodal status			**0.001**
N0	42	27	
N1 +	5		
Unknown	2	1	
Local recurrence			0.513
Yes		3	
No	47	46	

p-Values in bold print indicate statistical significance. *p*-Values were analyzed by chi-square test.

Table 2 Univariate and multivariate Cox regression models for estimating the overall survival

Characteristics	HR	95% CI	p-Value
Overall survival			
Univariate analysis			
Age (≥60 y vs <60 y)	2.937	0.890–4.5	0.093
Gender (male vs female)	2.584	0.858–3.975	0.108
Alcohol history (Alcohol none Alcohol)	1.914	0.5–3.529	0.363
Smoking history (smoker vs nonsmoker)	1.13	0.770–3.16	0.187
Histological grade (differentiation)	327	1.00–5.141	**0.038**
Tumor size (T3, T4 vs T1, T2)	1.1	56–2.877	0.400
Nodal status (N1+ vs N0)	23	1.140–5.0115	**0.021**
PTK7 expression (high vs low)	9.81	1.713–10.362	**0.002**
Multivariate analysis			
Histological grade (differentiation)	3.877	0.1193–2.995	**0.049**
Nodal status (N1+ vs N0)	5.41	1.150–5.159	**0.023**
PTK7 expression (high vs low)	9.286	1.654–10.153	**0.002**

HR hazard ratio, *CI* confidence interval. P-values in bold print indicate statistical significance

phenotype[24,25,35,36], and PTK7 has been shown to be a CSC marker in some tumors[7,8]. We efficiently knocked down PTK7 expression in the HN6 and SCC-25 cells and overexpressed PTK7 expression in CAL 27 cells with GFP-tagged lentivirus (Supplementary Figure 4A). Then, we assessed the effect of POSTN and PTK7 on the CSC-like phenotype of tumor cells and the RT-PCR analysis showed that PTK7 knockdown impaired the expression of the CSC markers CD166, SALL4, CD271, CD90, CD133, OCT-4, ALDH, SOX2, and NANOG in the HN6 and SCC-25 cells. After treatment with rhPOSTN, the CSC markers of the HN6 and SCC-25 shNC cells upregulated about 7–17-fold, but that in the shPTK7 cells only upregulated about 1–4-fold (Fig. 4a and Supplementary Figure 4B), suggesting that PTK7 might act as a receptor of POSTN in POSTN-promoting CSC marker expression. In addition, overexpression of PTK7 and treatment with rhPOSTN improved the expression of the CSC markers in CAL 27 cells about 2–5-fold and 4–9-fold, respectively. Moreover, the combination of PTK7 overexpression and rhPOSTN treatment led to mRNA expression levels of CSC markers increasing about 10–22-fold in CAL 27 (Supplementary Figure 4C). Simultaneously, sphere formation and colony formation were significantly decreased in the HN6 and SCC-25 shPTK7 cells compared with the shNC cells ($p < 0.01$). Treatment with rhPOSTN increased the sphere-forming and colony formation capacity of the shNCs, but not that of the shPTK7 cells (Figs. 4b, c; Supplementary Figure 4D and 4F). Moreover, PTK7 overexpression and rhPOSTN treatment in CAL 27 cells

colocalization of PTK7 and POSTN in human HNSCC tissues (Fig. 3e). Consistently, HN6 and CAFs co-culture system showed that POSTN secreted by CAFs colocalized with PTK7 (Fig. 3f). Collectively, these results indicated that POSTN secreted by CAFs colocalized and interacted with PTK7 in HNSCC.

POSTN secreted by CAFs promoted the CSC-like phenotype of HNSCC cells and PTK7 might act as a receptor

Many studies have reported that POSTN secreted by CAFs promoted tumor progression and the CSC-like

RETRACTED ARTICLE

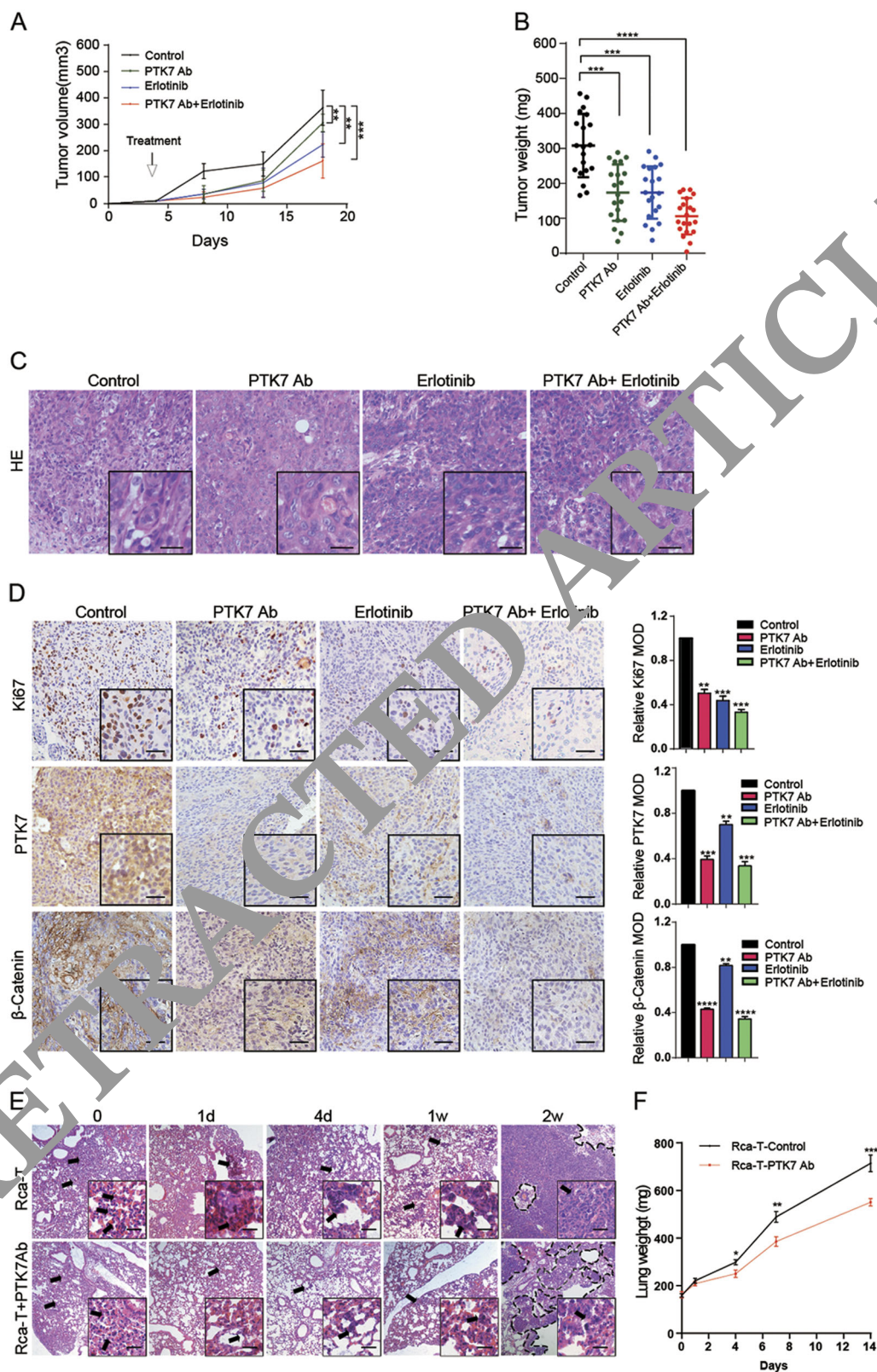**Fig. 2** (See legend on next page.)

Fig. 2 PTK7 inhibition enhanced erlotinib efficacy and reduced metastasis in vivo. a HN6 tumor-bearing mice were treated with vehicle, PTK7 antibody (10 μg per tumor nodule) around the tumor, erlotinib (50 mg/kg/day), or PTK7 antibody + erlotinib. After 14 days, the treatment was terminated; growth was monitored for a total of 18 days, and tumor volume was calculated. **b** The tumor weight of the HN6 tumor-bearing mice was calculated. **c** H& E staining of tumors from the HN6 tumor-bearing mice is shown. Scale bar: 10 μm. **d** Immunohistochemical analysis of PTK7, Ki67, and β-Catenin expression in tumor tissue sections from the BALB/C mice is shown. **p < 0.01, ***p < 0.001, ****p < 0.0001, based on Student's *t*-test. Scale bar: 10 μm. **e** H& E staining of lung tissue sections from BALB/C nude mice from the Rca-T and Rca-T + PTK7 antibody groups killed at 0, 1, and 4 days and 1 and 2 weeks is shown. Scale bar: 10 μm. **f** The lung weights of the Rca-T and Rca-T + PTK7 antibody groups at 0, 1, and 4 days and 1 and 2 weeks are shown. *p < 0.05, **p < 0.01, ***p < 0.001, based on Student's *t*-test

most significantly improved the sphere-forming and colony formation capacity (Supplementary Figure 4E and 4G). Consistent with the results in vivo, PTK7 knockdown significantly increased the sensitivity of the HN6 and SCC-25 cells to erlotinib (Fig. 4d and Supplementary Figure 4H). However, PTK7 overexpression in CAL 27 cells induced an almost 3-fold increase in resistance to erlotinib (Supplementary Figure 4I). The results of proliferation, migration, invasion, and motility assays were also similar to that of sphere-forming and colony formation capacity assays (Fig. 4e–h, Supplementary Figures 5A–5C and 6A–6D). Taken together, these findings suggested that POSTN secreted by CAFs promoted the CSC-like phenotype and the proliferation and invasion phenotype in HNSCC cells, and PTK7 might act as a receptor.

The POSTN–PTK7 axis promotes tumor growth and β-Catenin expression in HNSCC cells in vivo

To examine the effect of the POSTN–PTK7 axis on tumorigenicity in vivo, we established a xenograft model in BALB/C nude mice. The results demonstrated that the tumors comprising HN6 shPTK7 cells grew significantly slower than those comprising HN6 shNC cells (p < 0.001). Exogenous rhPOSTN significantly accelerated the tumor growth of the HN6 shNC cells (p < 0.01), but did not significantly accelerate the tumor growth of the HN6 shPTK7 cells (p > 0.05) (Figs. 5a, b and Supplementary Figure 6E). H&E staining did not demonstrate morphological differences in the xenograft tumors among HN6 shNC, HN6 shPTK7, HN6-NC-rhPOSTN, and HN6-shPTK7-rhPOSTN groups (Fig. 5c). The results of IHC assays showed that PTK7 knockdown reduced the proportion of Ki67- and β-Catenin-positive cells in the xenograft tumors and that rhPOSTN enhanced the proportion of Ki67- and β-Catenin-positive cells in the HN6 shNC cell population (Fig. 5d). Consistent with the in vitro data, these studies demonstrated that the POSTN–PTK7 axis promoted tumorigenicity and β-Catenin expression in HNSCC.

POSTN–PTK7 regulated Wnt/β-Catenin signaling in HNSCC

Considering that PTK7 serves as a catalyst for the Wnt pathway, we further investigated whether the POSTN–PTK7 influences the activation of Wnt/β-Catenin signaling. Western blot showed that the levels of p-LRP6, Dvl2, Naked2, p-GSK3β, and β-Catenin in the shNC cells markedly increased after rhPOSTN stimulation, but the HN6 and SCC-25 shPTK7 cells failed to activate Wnt/β-Catenin signaling. The expression level of GSK3β remained unchanged in both HN6 and SCC-25 cells (Figs. 6a, b). Correspondingly, rhPOSTN treatment also activated Wnt/β-Catenin signaling in the CAL 27 cells, and PTK7 overexpression enhanced the activation of Wnt/β-Catenin signaling (Fig. 6c). In addition, immunofluorescence showed that when the HN6 shNC cells were treated with rhPOSTN, β-Catenin translocated from the cytoplasm to the nucleus; however, β-Catenin remained in the cytoplasm in the HN6 shPTK7 cells (Fig. 6d). All these results indicated that POSTN activated Wnt/β-Catenin signaling by interacting with PTK7 (Fig. 6e).

Discussion

Although the treatment strategies for HNSCC have evolved much in recent years, high metastasis and recurrence rates result in unsatisfactory quality of life in patients with HNSCC[37]. CSCs are reported to play a major role in HNSCC persistence, metastasis, and recurrence, as well as in chemoresistance and radiation resistance[3,38,39]. Hence, understanding the mechanisms of HNSCC initiation, progression and the CSC-like phenotype may facilitate the development of future treatments.

We considered PTK7 as a new CSC surface marker for HNSCC as a result of our previous study[7]. PTK7 overexpression has been reported in multiple cancers[40–45], and previous reports have shown that an antibody-drug conjugate (ADC) targeting PTK7 was effective in treatment of triple-negative breast cancer, ovarian cancer, and non-small cell lung cancer[46,47]. In our study, we focused on detecting the cancer stemness and molecular mechanism of PTK7 in the initiation and progression of HNSCC instead of focusing on epidemiological results alone. Our data showed that PTK7 was highly expressed in HNSCC tissues and was associated with elevated Wnt/β-Catenin expression and poor clinical outcomes. Additionally, PTK7 inhibition enhanced erlotinib efficiency and reduced Wnt/β-Catenin expression and lung
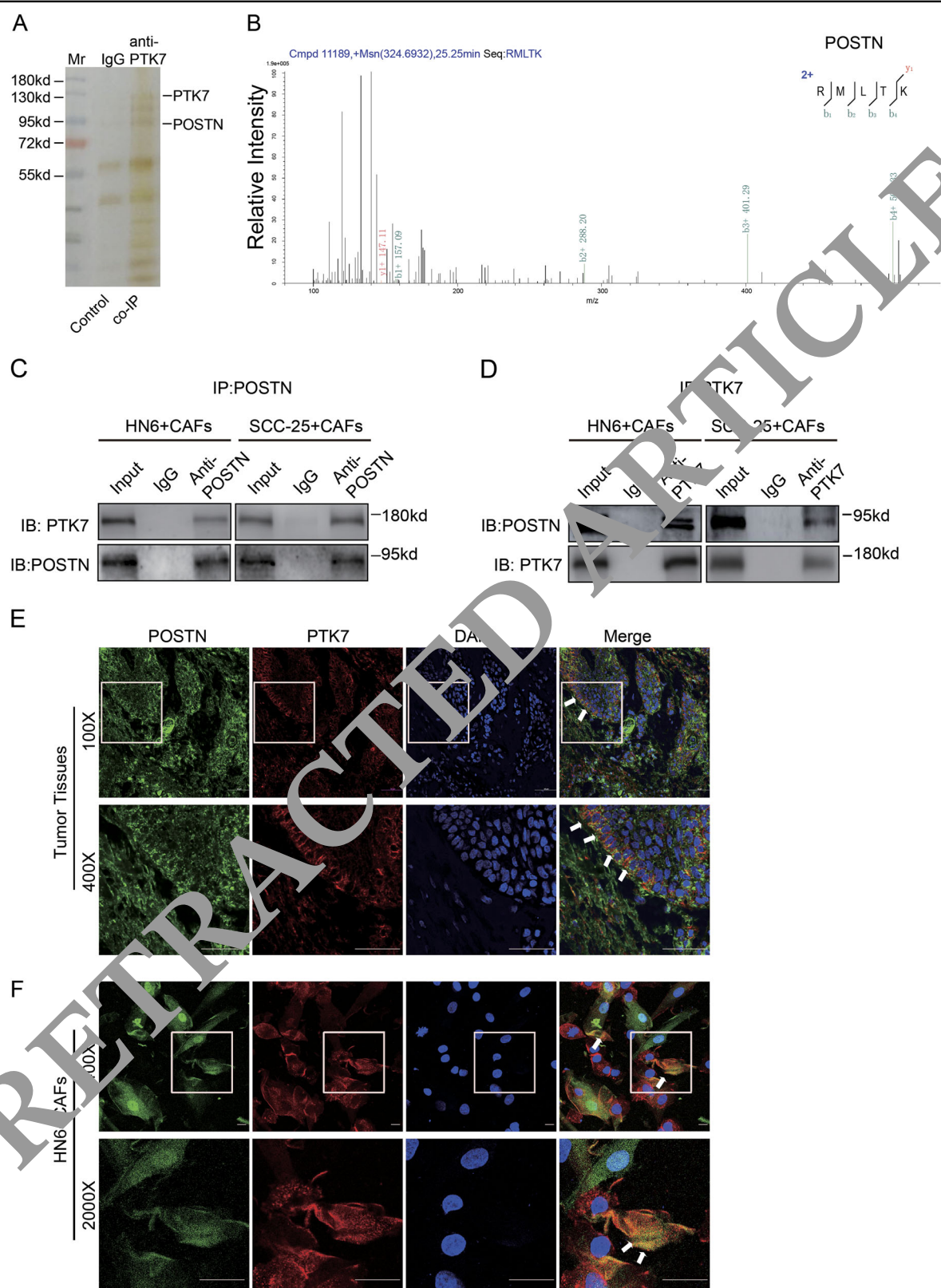
Fig. 3 (See legend on next page.)

(see figure on previous page)

Fig. 3 POSTN secreted by CAFs is a potential ligand of PTK7. a The eluates of the CAFs were subjected to co-IP with the PTK7 antibody, and the silver stain photo of control (IgG) and co-IP (anti-PTK7) group is shown. **b** The MS/MS spectrum of POSTN is shown. **c** Cell lysates from HN6 + CAFs and SCC-25 + CAFs were prepared and immunoprecipitated with IgG and anti-POSTN antibodies. The cell lysates and immunoprecipitates were analyzed by western blot with anti-PTK7 and anti-POSTN antibodies. **d** Cell lysates from HN6 + CAFs and SCC-25 + CAFs were prepared and immunoprecipitated with IgG and anti-PTK7 antibodies. The cell lysates and immunoprecipitates were analyzed by western blot with anti-PTK7 and anti-POSTN antibodies. **e** The localization of POSTN and PTK7 in the HNSCC tissues was detected by confocal laser scanning microscopy, as indicated. Scale bar: 50 μm. **f** The localization of POSTN and PTK7 in the co-cultured HN6 and CAFs cells was detected by confocal laser scanning microscopy, as indicated. Scale bar: 10 μm

metastasis in vivo. Therefore, PTK7 might be a prognostic and diagnostic biomarker for HNSCC.

Many reports have demonstrated that tumor progression and metastasis are joint effects of the tumor microenvironment and cancer cells[48,49]. CAFs are an important for creating different tumor components for cancer cells[50–53]. A previous study showed that CAFs secreted many factors that promote tumor initiation and progression[54]. This raised the question of why we focused on POSTN as the molecular link between tumor cells and CAFs. Our answer to this question has three parts. Firstly, our previous study reported that POSTN was mainly secreted by CAFs and played a major role in tumor growth and metastasis in HNSCC[29]. Secondly, many reports have demonstrated that POSTN promoted the CSC-like phenotype in tumors and was an upstream promoter of Wnt/β-Catenin signaling[24,26,55,56]. Thirdly, in this study, the MS results showed that PTK7 interacted with POSTN in CAFs. In addition, data from TCGA demonstrated that POSTN expression was positively correlated with PTK7 expression in HNSCC. Hence, we tried to explain the mechanism of the relationship among POSTN, PTK7, and Wnt/β-Catenin signaling. In this study, the data showed that POSTN significantly upregulated the CSC-like phenotype, proliferation, and invasion in HNSCC. However, PTK7 knockdown suppressed the function of POSTN. Therefore, we concluded that POSTN might play a major role in cancer stemness and tumor progression by interacting with PTK7 in HNSCC. The IHC results showed that POSTN was mainly located in the tumor stroma and that PTK7 was located mainly in cancer cells. This finding supports the opinion of the interaction between the tumor stroma and cancer cells and may facilitate the development of future treatments for HNSCC.

As previous reports have shown, the Wnt signaling pathway plays an important role in the normal development of tissues and organs[14,15,57], but abnormal activation might lead to cancer progression[58–61]. To understand the mechanism of this phenomenon, our study focused on Wnt/β-Catenin axis for two reasons. Firstly, PTK7 is known to be a receptor in Wnt signaling, and PTK7 knockdown inhibits Wnt/β-Catenin signaling[9,15]. Our data also demonstrated the positive correlation between PTK7 and Wnt/β-Catenin. Secondly, POSTN is reported to promote cancer stemness through Wnt/β-Catenin signaling. Hence, we supposed that POSTN and PTK7 have some molecular link involving the Wnt/β-Catenin axis. The results showed that secreted POSTN might bound to PTK7 on the cytomembrane, transduced signals to disheveled protein (Dvl2) through the cell surface receptor Lrp6, and reduced the phosphorylation of GSK3β and the hyperphosphorylation of β-Catenin, which caused β-Catenin to accumulate in the cytoplasm and enter the nucleus, suggesting that POSTN–PTK7 successfully activated the canonical Wnt signaling pathway. These results suggest that secreted POSTN plays an important role in the CSC-like phenotype and tumor progression in HNSCC. In addition, other studies reported that POSTN was also related to the integrinβ1/integrin αvβ3/AKT/Nanog/Notch pathway in addition to Wnt/β-Catenin signaling[24,26,62]. Therefore, it would be interesting to study the influence of POSTN–PTK7 on other signaling pathways.

In conclusion, this is the first time to demonstrate the relationship between POSTN and PTK7. Combination treatments targeting POSTN and PTK7 might be more effective, but further experiments should be performed to evaluate the exact mechanism of the interaction between these proteins and treatment efficiency in the future.

Materials and methods
Ethics statement

The tissue samples were collected from the Oral Cancer Tissue Bank of Shanghai, Affiliated with the Ninth People's Hospital of the Shanghai Jiao Tong University School of Medicine. The experiments were approved by the Clinical Research Ethics Committee of Ninth People's Hospital, Shanghai Jiao Tong University School of Medicine. All procedures were carried out in accordance with the approved guidelines of the Shanghai Jiao Tong University, and the studies were performed in accordance with the provisions of the Helsinki Declaration of 1975. All the patients involved in this study provided written informed consent, in accordance with institutional guidelines.
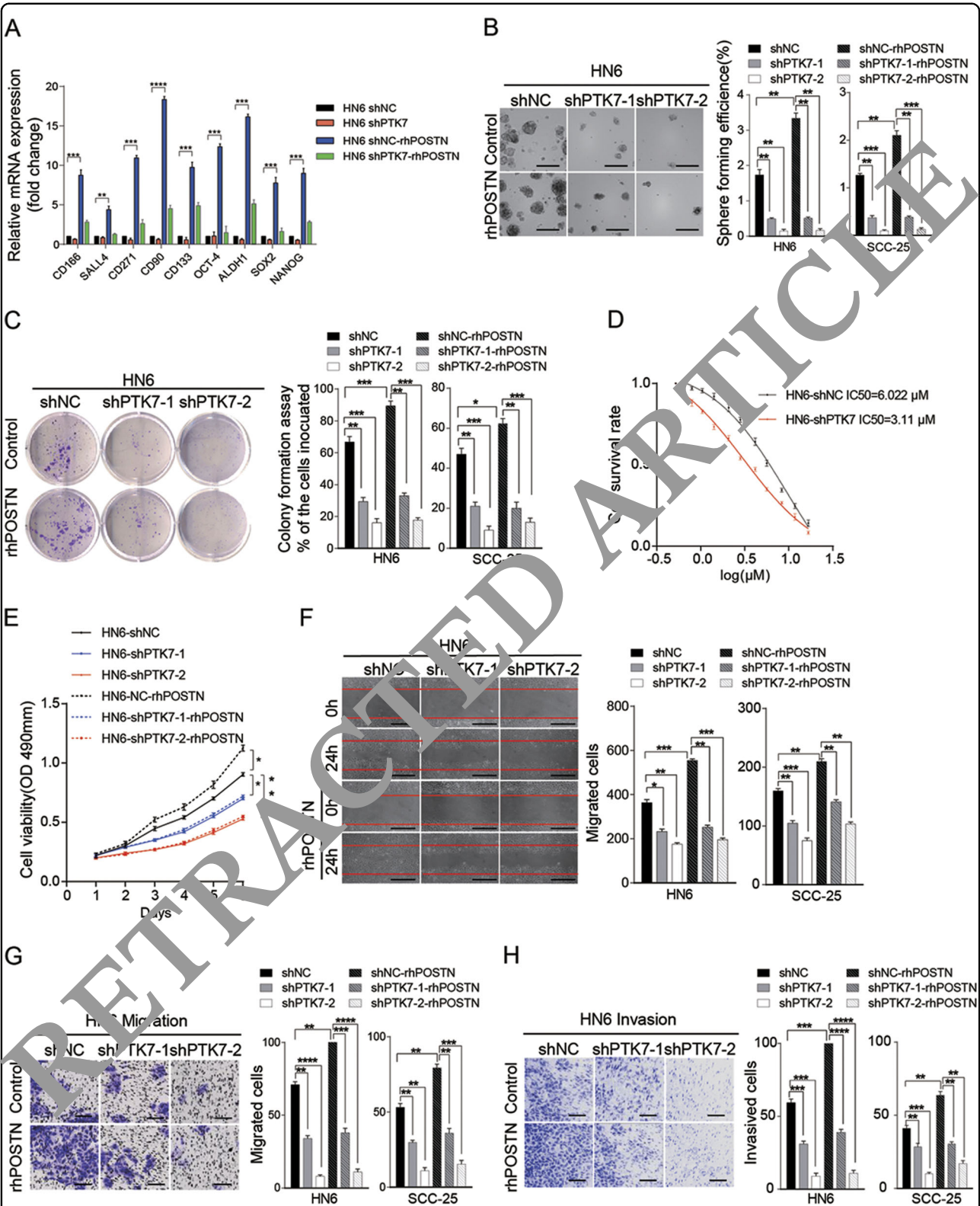
Fig. 4 (See legend on next page.)

(see figure on previous page)

Fig. 4 POSTN secreted by CAFs promotes the CSC-like phenotype and tumor initiation in HNSCC by interacting with PTK7. a After being starved with serum-free DMEM overnight, HN6 shNC and shPTK7 were exposed to rhPOSTN for 0 or 72 h, and the expression of the CSC markers CD166, SALL4, CD271, CD90, OCT-4, ALDH1, SOX2, and NANOG was analyzed by RT-PCR. **$p < 0.01$, ***$p < 0.001$, ****$p < 0.0001$, based on Student's *t*-test. **b** After being starved with serum-free DMEM overnight, HN6 shNC and shPTK7 were exposed to rhPOSTN for 0 or 72 h, and then their sphere-forming capacity was assessed. The results are shown as the mean ± SD. **$p < 0.01$, ***$p < 0.001$, based on Student's *t*-test. Scale bar: 20 μm. **c** After being starved with serum-free DMEM overnight, HN6 shNC and shPTK7 were exposed to rhPOSTN for 0 or 72 h, and then colony formation assay was performed. The results are shown as the mean ± SD. **$p < 0.01$, ***$p < 0.001$, based on Student's *t*-test. **d** After being starved with serum-free DMEM overnight, HN6 shNC and shPTK7 were exposed to erlotinib at different concentrations for 72 h. The IC$_{50}$ of erlotinib was evaluated on the basis of cell viability using CCK8 assay. **e** After being starved with serum-free DMEM overnight, HN6 shNC and shPTK7 were exposed to rhPOSTN for 0 or 72 h, and then proliferation assay was performed. The results are shown as the mean ± SD. *$p < 0.05$, **$p < 0.01$, based on Student's *t*-test. **f** After being starved with serum-free DMEM overnight, HN6 shNC and shPTK7 were exposed to rhPOSTN for 0 or 72 h, and then scratch-wound healing assay was performed. The results are shown as the mean ± SD. **$p < 0.01$, ***$p < 0.001$, based on Student's *t*-test. Scale bar: 40 μm. **g, h** After being starved with serum-free DMEM overnight, HN6 shNC and shPTK7 were exposed to rhPOSTN for 0 or 72 h, and then migration and invasion assay was performed. The results are shown as the mean ± SD. **$p < 0.01$, ***$p < 0.001$, ****$p < 0.0001$, based on Student's *t*-test. Scale bar: 50 μm

Cell cultures

Rca-T, NFs, CAFs, and five HNSCC cell lines, CAL 27, SCC-25, SCC-9, HN6, HN30 were used in these experiments[63].The human HNSCC cell lines HN6, HN30, SCC-9, SCC-25, and CAL 27 were obtained from the National Institutes of Health. The Rca-T cell line was purified from tongue squamous cell carcinoma tissues induced by adding 4-nitroquinoline-1-oxide into Sprague-Dawley rats' drinking water. NFs and CAFs were isolated from adjacent normal tissues and tumor tissues of HNSCC patients by primary culture. HN6, HN30, CAL 27, NFs, CAFs, and Rca-T were cultured in Dulbecco's modified Eagle's medium (DMEM; Gibco, Grand Island, NY, USA) containing 10% fetal bovine serum (FBS; Gibco, USA), 100 units/mL penicillin and 100 μg/mL streptomycin at 37 °C in a humidified 5% CO_2 atmosphere. SCC-9 and SCC-25 were cultured in DMEM/F12 media (Gibco, Waltham, MA, USA), containing 10% FBS (Gibco, USA), 100 units/mL penicillin and 100 μg/mL streptomycin at 37 °C in a humidified 5% CO_2 atmosphere.

Patients and samples

Tissue microarrays included 10 normal tissues and 101 primary HNSCC tissues from HNSCC patients who received surgery at the Department of Oral and Maxillofacial-Head and Neck Oncology, Ninth People's Hospital, Shanghai Jiao Tong University School of Medicine. Seventy-four pairs of HNSCC specimens (adjacent normal tissues and tumor tissues) were used for quantitative real-time PCR (qRT-PCR) and 12 pairs were used for western blot analysis. All patients wrote the informed consent and these studies were approved by the Ethics Boards of the Ninth People's Hospital.

IHC and Immunofluoresence

For IHC, we used tissue microarrays containing 101 HNSCC specimens and 10 normal tissues at Shanghai Ninth People's Hospital. One patient's tissues were removed from the study during IHC staining, and two patients had no follow-up information; thus, a total of 98 patients, including 66 patients who survived and 32 patients who died, remained in the study. Paraffin-embedded slides were deparafinized in graded xylene, rehydrated in graded ethanols, and then were heated with citric acid buffer for antigenic retrieval. The slides were cooled at room temperature and submerged into 0.3% hydrogen peroxide for 15 min to block endogenous peroxidase activity. After washed in phosphate-buffered saline (PBS) for 5 min, sections were blocked with 10% bovine serum albumin (BSA) at room temperature for 1 h. The indicated primary antibodies were incubated on the tissues in a humidified chamber at 4 °C overnight, and horseradish peroxidase (HRP)-labeled goat anti-mouse or goat anti-rabbit secondary antibody (Gene Tech, China) was incubated for 30 min at room temperature. Hematoxylin and dehydration were used to counterstain the nucleus. Then slides were submerged into graded ethanols and xylene and covered with coverslips. Primary antibodies were used at the following dilutions: rabbit polyclonal PTK7 antibody (Proteintech, 17799-1-AP, USA; 1:200), Mouse Monoclonal Ki67 antibody (Dako, China; 1:150), rabbit polyclonal β-Catenin antibody (Proteintech, 51067-2-AP, USA; 1:200). The histochemistry score (*H*-score) was quantified using a semi-automated computerized image analysis system (Quant Center; Pannoramic MIDI/P250, 3DHISTECH, Hungary), which was reported to analyze histological sections in previous studies[64–66]. $H\text{-score} = \Sigma(\text{PI} \times I) =$ (percentage of cells of weak intensity × 1) + (percentage of cells of moderate intensity × 2) + (percentage of cells of strong intensity × 3). I represents the intensity of staining and PI represents percentage of stained tumor cells. The *H*-score was independently assessed by two assessors who were not aware of the clinical outcomes. In this study, the median PTK7 *H*-score for all samples was 121.4275, which was the cutoff value for PTK7 low or high

expression. Therefore, *H*-score <121.4275 was considered low expression and H-score >121.4275 was considered high expression.

For tissues immunofluoresence, after incubated with primary antibodies (PTK7, Proteintech, 17799-1-AP, USA; 1:200; POSTN, Proteintech, 19899-1-AP, USA; 1:200), tissue sections were incubated with SignalStain® Boost IHC detection Reagent (HRP rabbit, #8114, CST or HRP mouse, #8125, CST) in a humidified chamber at room temperature for 30 min, protected from light. Fluorophore-conjugated TSA® Plus Amplification Reagent (NEL760001KT) was diluted as per the manufacturer's recommendation and incubated for 10 min at room temperature in a humidified chamber, protected from light. After wash three times, mount sections was covered with coverslips using ProLong® Gold Antifade Reagent with DAPI (CST, #8961).

For cells immunofluoresence, cells grew on coverslips, washed three times, fixed in 4% paraformaldehyde, permeabilized with 0.1% Triton X-100, and incubated with primary antibodies (PTK7; Proteintech, 17799-1-AP, USA; 1:200; β-Catenin, Proteintech, 51067-2-AP, USA; 1:200) at 4 °C overnight. Cells were incubated with secondary antibody (HRP rabbit, #8114, CST) and stained with Fluorophore-conjugated TSA® Plus amplification reagent (NEL760001KT), then covered with coverslips using ProLong® Gold Antifade Reagent with DAPI (CST, #8961).

Real-time PCR

Total RNA was extracted with TRIzol Reagent (Invitrogen, USA) according to the manufacturer's protocol and subsequently reverse transcribed into cDNA using the PrimerScript RT reagent Kit (Takara, Japan). The cDNA was amplified using the SYBR Premix Ex Taq reagent kit (Takara, Japan) according to the protocol. All the real-time PCR reactions were performed with an ABI StepOne real-time PCR system (Life Technologies, USA). Specific primers for PCR were provided in Table 3.
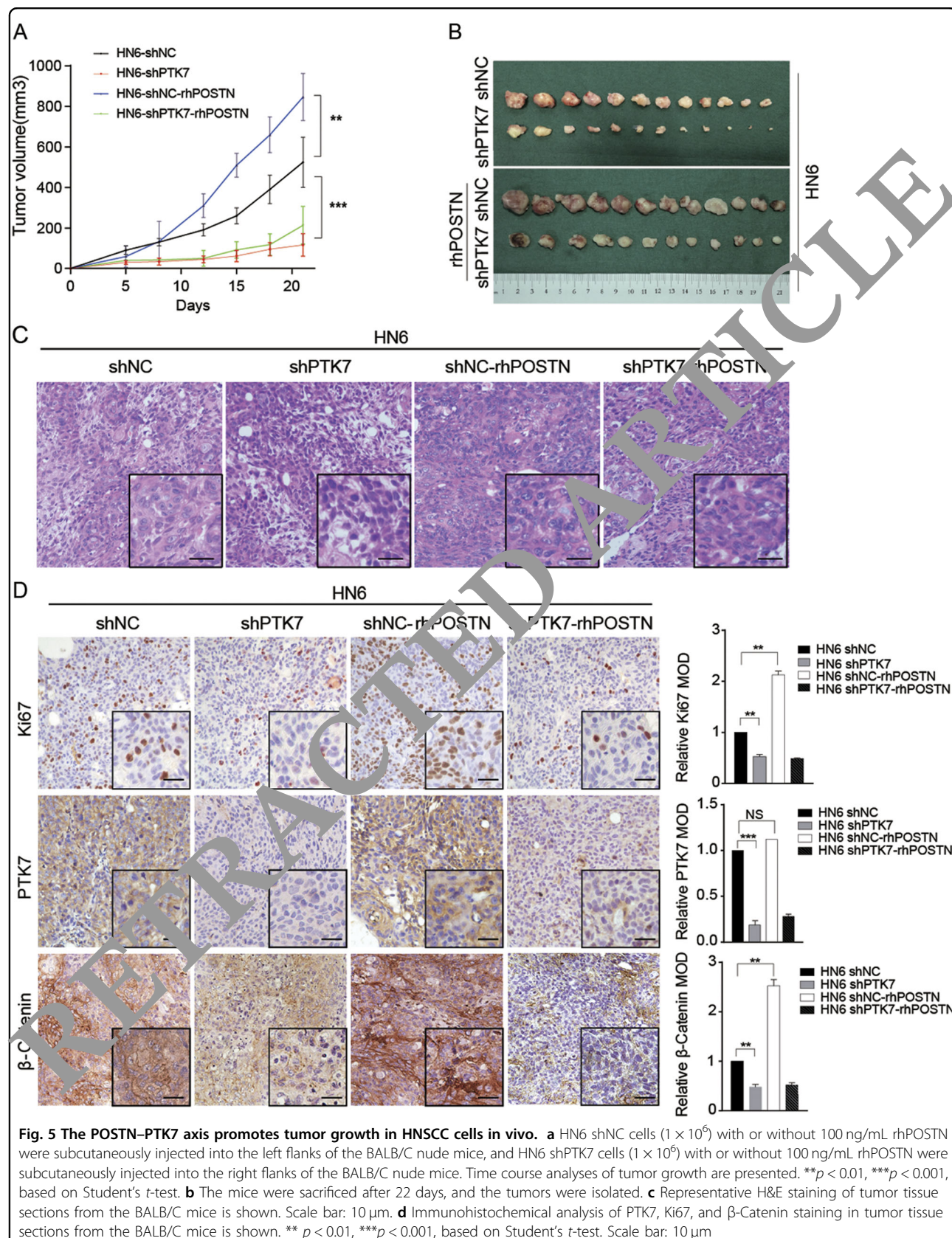
Western blot analysis

HNSCC cells or tissues were harvested in RIPA lysis buffer (Yeasen, China) and whole-cell lysate was electrophoresed using sulfate-polyacrylamide gel electrophoresis (SDS-PAGE), transferred to a polyvinylidene fluoride (PVDF) membrane, blocked with non-fat milk for 1 h at room temperature, and probed with primary antibodies: a rabbit polyclonal PTK7 antibody (Proteintech, 17799-1-AP, USA; 1:1000), a rabbit monoclonal p-Lrp6 antibody (CST, #2568, USA; 1:1000), a rabbit monoclonal Dvl2 antibody (CST, #3224, USA; 1:1000), a rabbit monoclonal Naked2 antibody (CST, #2073, USA; 1:1000), a rabbit monoclonal GSK3β antibody (Proteintech, 22104-1-AP, USA; 1:1000), a rabbit polyclonal p-GSK3β antibody (Signalway antibody, #11002, USA; 1:1000), a rabbit polyclonal β-Catenin antibody (Proteintech, 51067-2-AP, USA; 1:1000), a rabbit polyclonal E-cadherin antibody (Proteintech, 20874-1-AP, USA; 1:1000), a rabbit polyclonal Vimentin antibody (Proteintech, 10366-1-AP, USA; 1:1000), a rabbit polyclonal alpha-Tubulin Polyclonal antibody (Proteintech, 11224-1-AP, USA; 1:1000) overnight at 4 °C and then with rabbit or mouse HRP-linked secondary antibodies (CST, USA; 1:10000) and visualized with ECLUltra (New Cell and Molecular Biotech, Suzhou, China).
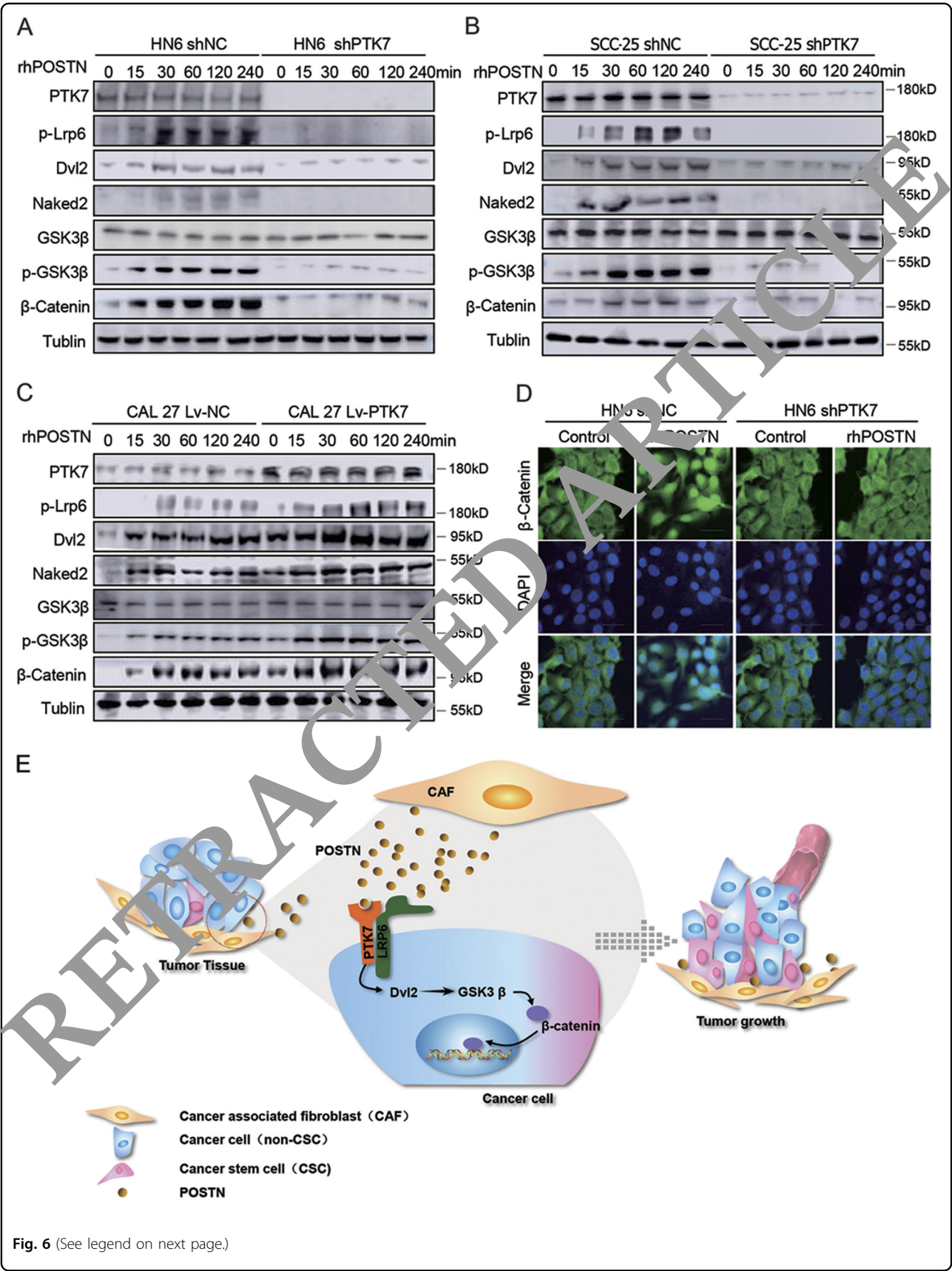
Protein silver stain and co-IP assay

Protein sliver stain and co-IP Assay was performed using the Pierce Classic IP Kit (Thermo Scientific). To

Table 3   Primers used in PCR

Gene name	Forward primer	Reverse primer
PTK7	CAGTTCCTGAGGATTTCCAAGAG	TGCATAGGGCCACCTTC
GAPDH	ACAACTTTGGTATCGTGGAAGG	GCCATCACGCCACAGTTTC
CD166	ACGATGAGGCAGACGAGATAAG	ATGCAGTCTTTGACTTCTTCATGT
SALL	AGCACATCAACTCGGAGGAG	CATTCCCTGGGTGGTTCACTG
CD271	CCTACGGCTACTACCAGGATG	CACACGGTGTTCTGCTTGT
CD90	ATCGCTCTCCTGCTAACAGTC	CTCGTACTGGATGGGTGAACT
CD133	AGTCGGAAACTGGCAGATAGC	GGTAGTGTTGTACTGGGCCAAT
OCT-4	CTTGAATCCCGAATGGAAAGGG	GTGTATATCCCAGGGTGATCCTC
ALDH1	GCACGCCAGACTTACCTGTC	CCTCCTCAGTTGCAGGATTAAAG
SOX2	GCCGAGTGGAAACTTTTGTCG	GGCAGCGTGTACTTATCCTTCT
NANOG	TTTGTGGGCCTGAAGAAAACT	AGGGCTGTCCTGAATAAGCAG

Fig. 5 The POSTN–PTK7 axis promotes tumor growth in HNSCC cells in vivo. **a** HN6 shNC cells (1×10^6) with or without 100 ng/mL rhPOSTN were subcutaneously injected into the left flanks of the BALB/C nude mice, and HN6 shPTK7 cells (1×10^6) with or without 100 ng/mL rhPOSTN were subcutaneously injected into the right flanks of the BALB/C nude mice. Time course analyses of tumor growth are presented. **$p < 0.01$, ***$p < 0.001$, based on Student's *t*-test. **b** The mice were sacrificed after 22 days, and the tumors were isolated. **c** Representative H&E staining of tumor tissue sections from the BALB/C mice is shown. Scale bar: 10 μm. **d** Immunohistochemical analysis of PTK7, Ki67, and β-Catenin staining in tumor tissue sections from the BALB/C mice is shown. ** $p < 0.01$, ***$p < 0.001$, based on Student's *t*-test. Scale bar: 10 μm

Fig. 6 (See legend on next page.)

Fig. 6 POSTN–PTK7 regulated Wnt/β-Catenin signaling in HNSCC. a After being starved with serum-free DMEM overnight, HN6 shNC and shPTK7 cells were treated with 100 ng/mL rhPOSTN for 0, 15, 30, 60, 120, 240 min. The lysates were prepared, and the expression of PTK7, p-Lrp6, Dvl2, Naked2, GSK3β, p-GSK3β, and β-Catenin was analyzed by western blot. Tubulin was used as a loading control. **b** After being starved with serum-free DMEM overnight, SCC-25 shNC and shPTK7 cells were treated with 100 ng/mL rhPOSTN for 0, 15, 30, 60, 120, and 240 min. The lysates were prepared, and the expression of PTK7, p-Lrp6, Dvl2, Naked2, GSK3β, p-GSK3β, and β-Catenin was analyzed by western blot. Tubulin was used as a loading control. **c** After being starved with serum-free DMEM overnight, CAL 27 Lv-NC and Lv-PTK7 cells were treated with 100 ng/mL rhPOSTN for 0, 15, 30, 60, 120, and 240 min. The lysates were prepared, and the expression of PTK7, p-Lrp6, Dvl2, Naked2, GSK3β, p-GSK3β, and β-Catenin was analyzed by western blot. Tubulin was used as a loading control. **d** After being starved with serum-free DMEM overnight, HN6 shNC and shPTK7 cells were treated with control DMEM medium or 100 ng/mL rhPOSTN for 30 min; the location of β-Catenin was detected by laser scanning microscopy. Scale bar: 10 µm

detect whether PTK7 act with proteins in CAFs, CAFs were rinsed with cold PBS and lysed in the IP Lysis for 5 min, subsequently centrifuged at 13,000 rpm for 10 min to pellet the cell debries. Control agarose slurry was added into the lysate to remove non-specificity integration and primary antibody (PTK7, Proteintech, 17799-1-AP) or control IgG (CST, #2729) was added to the lysates at 4 °C overnight. After washing three times, the antibody/lysate mixture was captured by the Pierce Protein A/G Agarose and then detected by electrophoresis.

For protein sliver stain, gel was fixed in 10% acetic acid +40% ethyl alcohol for 120 min, and then was sensitized in sensitization liquid for 60 min at room temperature. After washing three times for 30 min, gel was submerged into 0.1% silver nitrate for 60 min. The gel was washed for another four times and developed color until desired intensity of staining occurs. Terminate the color development and wash the gel for permanent storage. All steps used the Protein Sliver Stain Kit (Yeason, China).

For co-IP Assay, the antibody/lysate mixture was captured by the Pierce Protein A/G Agarose and then detected by western blot according to the manufacturer's protocols. To further evaluate the exact interaction between POSTN and PTK7, HN6 or SCC-25 cells were co-cultured with CAFs and POSTN (Abcam, ab219056), PTK7 (Proteintech, 17799-1-AP), or control IgG (CST, #2729) was added the the lysaste mixture at 4 °C overnight. After washing three times, the antibody/lysaste mixture was captured by the Pierce Protein A/G Agarose and then detected by western blot according to manufacture's protocols.

MS analysis

The proteins in gel of control and the co-IP after silver stain were reduced in DTT for 1 h at 56 °C and were alkylated by a solution of 55 mM iodoacetamide in the dark for 1 h at room temperature. Trypsin (12.5 ng/L in 25 mM NH_4HCO_3, pH 8.0) was added to each gel piece at 37 °C for 20 h. Then the peptides were extracted twice with 50% acetonitrile/0.5% formic acid and combined

extracts were dried in a SpeedVac instrument for subsequent LC-MS/MS analysis. The peptides were separated using a Q Exactive mass spectrometer coupled to Easy nLC (ProxeonBiosystems, now Thermo Fisher Scientific). The peptides were loaded with 95% solvent A (10 mM ammonium formate, pH 10 in 95:5 water:acetonitrile) and solvent B (10 mM ammonium formate, pH 10 in 16:84 water:acetonitrile). A stepwise gradient of 0–55% solvent B for 83–85 min and 55–100% solvent B for 85–95 min was used to separate the peptides. Survey scans were set at a resolution of 70,000 at 200m/z and resolution for HCD spectra was 17,500 at 200m/z. Normalized collision energy was 30 eV and dynamic exclusion duration was 60 s. MS/MS spectra were used to search with the MASCOT engine (Matrix Science, London, UK; version 2.2) using the nonredundant UniProt International Protein Index. The parameters were provided in Supplement Table 3.

Lentivirus transfection

For gene silencing, HN6 and SCC-25 cells were transfected with GFP-labeled shPTK7 lentivectors or control lentivectors (Genomeditech, Shanghai, China) according to the manufacturer's instruction. Similarly, CAL 27 cell line was transfected with lentiviral particles with PTK7 construct or empty vector (Genomeditech, Shanghai, China). Rca-T cells were transfected with with GFP-labeled lentivectors. Then the cells were treated with puromycin (5 µg/mL) for 2 weeks to establish stable cell lines.

Sphere-forming assay

A single-cell suspension of 1×10^5 HNSCC cells was seeded in ultra-low attachment six-well plates (Corning, USA). Cells were cultured in DMEM/F12 media (Gibco, USA) supplemented with 20 ng/mL bFGF, 20 ng/mL EGF, 1% N2, 2% B27 (Gibco, USA). The culture media was changed twice a day until the diameter of the sphere reached 0.5 mm. The number of spheres was calculated 2 weeks after seeding. Each assay was repeated at least three times.

Cell proliferation assay

HNSCC cells were plated in 96-well plates at a density of 1×10^3 cells per well. At the indicated time points, 10% CCK8 (Dojindo, Japan) was added to the plate and the OD value at 450 nm was measured after 1–4 h. All experiments were performed in triplicate, and the mean proliferation rate was reported.

Colony formation assay

HNSCC cells were plated in six-well plates at a density of 1×10^3 cells per well in triplicate, and cultured in a humidified incubator at 37 °C. After 2 weeks, cells were washed with PBS, fixed in 4% paraformaldehyde, stained with 0.5% crystal violet, and were counted at least three times.

Transwell assay

For cell migration assay, a total of 2×10^4 HNSCC cells in 200 μL serum-free DMEM was plated in the upper chamber (Merck Millipore, USA) of the 24-well plates and 600 μL DMEM or DMEM/F12 containing 10% FBS with or without 100 ng/mL rhPOSTN was added to the lower chamber of 24-well plates. After cultured in a humidified incubator at 37 °C for 24 h, the chamber was washed with PBS for three times, fixed in 4% paraformaldehyde, stained with 0.5% crystal violet for 1 h. Cells on the upper surface of the chamber were removed with a small cotton swab and washed under flowing water. After drying, cells were counted for at least three times.

For cell invasion assay, Matrigel (BD Biosciences, USA) was plated on the upper chamber at 37 °C overnight, and subsequent steps were the same as transwell invasion assay.

Wound-healing assay

HNSCC cells were cultured in six-well plates in DMEM or DMEM/F12 until 100% confluence. The cells were scraped with a P200 tip (red), washed with PBS for three times, changed to serum-free DMEM with or without 100 ng/mL rhPOSTN, and pictures were taken at 0, 12, and 24 h for at least five non-overlapping fields.

Animal experiments

All animal experiments were performed in accordance with the guidelines approved by the Shanghai Jiao Tong University School of Medicine. To determine the role of PTK7 in chemoresistance, a total of 1×10^6 HN6 cells in 100 μL serum-free DMEM were subcutaneously injected into the left and right flanks of the 6-week-old BALB/C nude mice. Four days after injection, the tumor-bearing mice (20 tumors each group) were treated with vehicle, PTK7 antibody (10 μg per tumor nodule) around the tumor, erlotinib (50 mg/kg/day), or the combination of PTK7 antibody and erlotinib (50 mg/kg/day) twice a day for 14 days.

To determine the role of PTK7 in lung metastasis, the lung metastasis model was performed. A total of 2×10^6 Rca-T cells in 200 μL serum-free DMEM with or without PTK7 antibody was injected intravenously into the lateral tail vein of the 6-week-old BALB/C nude mice (3 mice each group). The animals were sacrificed at 0, 1, and 4 days and 1 and 2 weeks respectively. In every group, one lung tissues was performed cryosections and the other two were fixed in neutral-buffered formalin for further experiments. Tumor volume $= 1/2 \times$ length $\times$ (width)^2. Mice were sacrificed at day 18 and tumors were isolated.

To evaluate the tumor-promoting role of POSTN and PTK7 in vivo, a xenograft model was performed in BALB/C nude mice about 6-week old. 1×10^6 HN6 shNC or HN6 shPTK7 cells in 100 μL serum-free DMEM with or without 100 ng/mL rhPOSTN were injected subcutaneously into the left or right posterior flanks of the BALB/C nude mice. The weight of the mice and tumor volume were measured every third day for a total of over 20 days. Mice were sacrificed at day 22 and tumors were taken out and photographed. After formalin submerged and paraffin embedded, the tissues were performed H&E and IHC experiments.

Statistical analyses

All of the measurement data were performed with SPSS 19.0 statistical software. Kaplan–Meier survival analyses were used to analyze the relationship between PTK7 expression level and the clinicopathologic features. Student's *t*-test and one-way ANOVA were used to compare the means of two or more groups. The Cox proportional hazards model was used for multivariate analyses; $p < 0.05$ was considered to be statistically significant.

Author details
[1]Department of Oral and Maxillofacial-Head & Neck Oncology, Shanghai Ninth People's Hospital & College of Stomatology, Shanghai Jiao Tong University School of Medicine, Shanghai 200011, China. [2]National Clinical Research Center of Stomatology, Shanghai Key Laboratory of Stomatology & Shanghai Research Institute of Stomatology, Shanghai 200011, China. [3]Department of Oral Pathology, Shanghai Ninth People's Hospital, Shanghai Jiao Tong University School of Medicine, Shanghai 200011, China

Conflict of interest
The authors declare that they have no conflict of interest.

Publisher's note
Springer Nature remains neutral with regard to jurisdictional claims in published maps and institutional affiliations.

Supplementary Information accompanies this paper at (https://doi.org/10.1038/s41419-018-1116-6).

References

1. Torre, L. A. et al. 1 Global cancer statistics, 2012. *CA Cancer J. Clin.* **65**, 87–108 (2015).
2. D'Cruz, A. K. et al. Elective versus therapeutic neck dissection in node-negative oral cancer. *N. Engl. J. Med.* **373**, 521–529 (2015).
3. Chen, D. et al. Targeting BMI1(+) cancer stem cells overcomes chemoresistance and inhibits metastases in squamous cell carcinoma. *Cell Stem Cell* **20**, 621–634.e626 (2017).
4. Li, P. et al. CRB3 downregulation confers breast cancer stem cell traits through TAZ/beta-catenin. *Oncogenesis* **6**, e322 (2017).
5. Li, C. et al. CD54-NOTCH1 axis controls tumor initiation and cancer stem cell functions in human prostate cancer. *Theranostics* **7**, 67–80 (2017).
6. Brabletz, T., Jung, A., Spaderna, S., Hlubek, F. & Kirchner, T. Opinion: migrating cancer stem cells—an integrated concept of malignant tumour progression. *Nat. Rev. Cancer* **5**, 744–749 (2005).
7. Yan, M. et al. Plasma membrane proteomics of tumor spheres identify CD166 as a novel marker for cancer stem-like cells in head and neck squamous cell carcinoma. *Mol. Cell Proteomics* **12**, 3271–3284 (2013).
8. Jung, P. et al. Isolation of human colon stem cells using surface expression of PTK7. *Stem Cell Rep.* **5**, 979–987 (2015).
9. Liu, Q. et al. PTK7 regulates Id1 expression in CD44-high glioma cells. *Neuro-Oncol.* **17**, 505–515 (2015).
10. Dong, Y. et al. PTK7 is a molecular marker for metastasis, TNM stage, and prognosis in oral tongue squamous cell carcinoma. *Pol. J. Pathol.* **68**, 49–54 (2017).
11. Puppo, F. et al. Protein tyrosine kinase 7 has a conserved role in Wnt/beta-catenin canonical signalling. *EMBO Rep.* **12**, 43–49 (2011).
12. Hayes, M. et al. ptk7 mutant zebrafish models of congenital and idiopathic scoliosis implicate dysregulated Wnt signalling in disease. *Nat. Commun.* **5**, 4777 (2014).
13. Hayes, M., Naito, M., Daulat, A., Angers, S. & Ciruna, B. Ptk7 promotes non-canonical Wnt/PCP-mediated morphogenesis and inhibits Wnt/beta-catenin-dependent cell fate decisions during vertebrate development. *Development* **140**, 1807–1818 (2013).
14. Berger, H., Wodarz, A. & Borchers, A. PTK7 faces the Wnt in development and disease. *Front. Cell Dev. Biol.* **5**, 31 (2017).
15. Bin-Nun, N. et al. PTK7 modulates Wnt signaling activity via LRP6. *Development* **141**, 410–421 (2014).
16. Xian, L. et al. HMGA1 amplifies Wnt signalling and expands the intestinal stem cell compartment and Paneth cell niche. *Nat. Commun.* **8**, 15008 (2017).
17. Kim, J. H., Park, S. Y., Jun, Y., Kim, J. Y. & Nam, J. S. Roles of Wnt target genes in the journey of cancer stem cells. *Int. J. Mol. Sci.* **18**, E1604 (2017).
18. Fu, L. et al. Wnt2 secreted by tumour fibroblasts promotes tumour progression in oesophageal cancer by activation of the Wnt/beta-catenin signalling pathway. *Gut* **60**, 1635–1643 (2011).
19. Xu, X. et al. Periostin expression in intra-tumoral stromal cells is prognostic and predictive for colorectal carcinoma via creating a cancer-supportive niche. *Oncotarget* **7**, 798–813 (2016).
20. Oskarsson, T. & Massague, J. Extracellular matrix players in metastatic niches. *EMBO J.* **31**, 254–256 (2012).
21. Cui, D., Huang, Z., Liu, Y. & Ouyang, G. The multifaceted role of periostin in priming the tumor microenvironments for tumor progression. *Cell. Mol. Life Sci.* **74**, 4287–4291 (2017).
22. Bao, S. et al. Periostin potently promotes metastatic growth of colon cancer by augmenting cell survival via the Akt/PKB pathway. *Cancer Cell.* **5**, 329–339 (2004).
23. Shi, Y., Ping, Y. F., Zhang, X. & Bian, X. W. Hostile takeover: glioma stem cells recruit TAMs to support tumor progression. *Cell Stem Cell* **16**, 219–220 (2015).
24. Zhang, R. et al. Activated hepatic stellate cells secrete periostin to induce stem cell-like phenotype of residual hepatocellular carcinoma cells after heat treatment. *Sci. Rep.* **7**, 2164 (2017).
25. Malanchi, I. et al. Interactions between cancer stem cells and their niche govern metastatic colonization. *Nature* **481**, 85–89 (2011).
26. Zhou, W. et al. Periostin secreted by glioblastoma stem cells recruits M2 tumour-associated macrophages and promotes malignant growth. *Nat. Cell Biol.* **17**, 170–182 (2015).

27. Zhang, F. et al. Periostin: a downstream mediator of EphB4-induced osteogenic differentiation of human bone marrow-derived mesenchymal stem cells. *Stem Cells Int.* **2016**, 7241829 (2016).
28. Lv, J. et al. Involvement of periostin-sclerostin-Wnt/beta-catenin signaling pathway in the prevention of neurectomy-induced bone loss by naringin. *Biochem. Biophys. Res. Commun.* **468**, 587–593 (2015).
29. Qin, X. et al. TGFbeta3-mediated induction of Periostin facilitates head and neck cancer growth and is associated with metastasis. *Sci. Rep.* **6**, 20587 (2016).
30. Lee, T. K. et al. CD24(+) liver tumor-initiating cells drive self-renewal and tumor initiation through STAT3-mediated NANOG regulation. *Cell Stem Cell* **9**, 50–63 (2011).
31. Lin, C. et al. Elevated RET expression enhances EGFR activation and mediates EGFR inhibitor resistance in head and neck squamous cell carcinoma. *Cancer Lett.* **377**, 1–10 (2016).
32. Ma, H. et al. Interferon-alpha enhances the antitumour activity of EGFR-targeted therapies by upregulating RIG-I in head and neck squamous cell carcinoma. *Br. J. Cancer* **118**, 509–521 (2018).
33. Soulieres, D. et al. Multicenter phase II study of erlotinib, an oral epidermal growth factor receptor tyrosine kinase inhibitor, in patients with recurrent or metastatic squamous cell cancer of the head and neck. *J. Clin. Oncol.* **22**, 77–85 (2004).
34. Yao, M. et al. Phase II study of erlotinib and docetaxel with concurrent intensity-modulated radiotherapy in locally advanced head and neck squamous cell carcinoma. *Head Neck* **38**(Suppl. 1), E1770–E1776 (2016).
35. Morra, L. & Moch, H. Periostin expression and epithelial-mesenchymal transition in cancer: a review and an update. *Virchows Arch.* **459**, 465–475 (2011).
36. Tian, B., Zhang, Y. & Zhang, J. Periostin is a new potential prognostic biomarker for glioma. *Tumour Biol.* **35**, 5877–5883 (2014).
37. Gross, A. M. & Orosco, R. K. Multi-tiered genomic analysis of head and neck cancer ties TP53 mutation to 3p loss. *Nat. Genet.* **46**, 939–943 (2014).
38. Chen, G., Jun, M., Li, R. R. & Chen, W. T. Sonic hedgehog signalling activation contributes to ALCAM over-expression and poor clinical outcome in patients with oral squamous cell carcinoma. *Chin. J. Dent. Res.* **21**, 31–40 (2018).
39. Wang, C., Liu, X. Q., Hou, J. S., Wang, J. N. & Huang, H. Z. Molecular mechanisms of chemoresistance in oral cancer. *Chin. J. Dent. Res.* **19**, 25–33 (2016).
40. Tian, X. et al. PTK7 overexpression in colorectal tumors: clinicopathological correlation and prognosis relevance. *Oncol. Rep.* **36**, 1829–1836 (2016).
41. Lin, Y. et al. PTK7 as a novel marker for favorable gastric cancer patient survival. *J. Surg. Oncol.* **106**, 880–886 (2012).
42. Gartner, S. et al. PTK 7 is a transforming gene and prognostic marker for breast cancer and nodal metastasis involvement. *PLoS ONE* **9**, e84472 (2014).
43. Jin, J., Ryu, H. S., Lee, K. B. & Jang, J. J. High expression of protein tyrosine kinase 7 significantly associates with invasiveness and poor prognosis in intrahepatic cholangiocarcinoma. *PLoS ONE* **9**, e90247 (2014).
44. Golubkov, V. S. & Strongin, A. Y. Downstream signaling and genome-wide regulatory effects of PTK7 pseudokinase and its proteolytic fragments in cancer cells. *Cell Commun. Signal.* **12**, 15 (2014).
45. Chen, R. et al. A meta-analysis of lung cancer gene expression identifies PTK7 as a survival gene in lung adenocarcinoma. *Cancer Res.* **74**, 2892–2902 (2014).
46. Damelin, M. et al. A PTK7-targeted antibody-drug conjugate reduces tumor-initiating cells and induces sustained tumor regressions. *Sci. Transl. Med.* **9**, pii: eaag2611 (2017).
47. Katoh, M. Canonical and non-canonical WNT signaling in cancer stem cells and their niches: cellular heterogeneity, omics reprogramming, targeted therapy and tumor plasticity (Review). *Int. J. Oncol.* **51**, 1357–1369 (2017).
48. Mittal, V. et al. The microenvironment of lung cancer and therapeutic implications. *Adv. Exp. Med. Biol.* **890**, 75–110 (2016).
49. Quail, D. F. & Joyce, J. A. Microenvironmental regulation of tumor progression and metastasis. *Nat. Med.* **19**, 1423–1437 (2013).
50. Labernadie, A. et al. A mechanically active heterotypic E-cadherin/N-cadherin adhesion enables fibroblasts to drive cancer cell invasion. *Nat. Cell Biol.* **19**, 224–237 (2017).
51. Affo, S., Yu, L. X. & Schwabe, R. F. The role of cancer-associated fibroblasts and fibrosis in liver cancer. *Annu. Rev. Pathol.* **12**, 153–186 (2017).
52. Marsh, T., Pietras, K. & McAllister, S. S. Fibroblasts as architects of cancer pathogenesis. *Biochim. Biophys. Acta* **1832**, 1070–1078 (2013).
53. Ostman, A. & Augsten, M. Cancer-associated fibroblasts and tumor growth--bystanders turning into key players. *Curr. Opin. Genet. Dev.* **19**, 67–73 (2009).
54. Kalluri, R. & Zeisberg, M. Fibroblasts in cancer. *Nat. Rev. Cancer* **6**, 392–401 (2006).

55. Zhang, F. et al. Periostin upregulates Wnt/beta-catenin signaling to promote the osteogenesis of CTLA4-modified human bone marrow-mesenchymal stem cells. *Sci. Rep.* **7**, 41634 (2017).

56. Bonnet, N., Conway, S. J. & Ferrari, S. L. Regulation of beta catenin signaling and parathyroid hormone anabolic effects in bone by the matricellular protein periostin. *Proc. Natl. Acad. Sci. USA* **109**, 15048–15053 (2012).

57. Boras-Granic, K. & Wysolmerski, J. J. Wnt signaling in breast organogenesis. *Organogenesis* **4**, 116–122 (2008).

58. Ma, J., Lu, W., Chen, D., Xu, B. & Li, Y. Role of Wnt co-receptor LRP6 in triple negative breast cancer cell migration and invasion. *J. Cell Biochem.* **118**, 2968–2976 (2017).

59. Tammela, T. et al. A Wnt-producing niche drives proliferative potential and progression in lung adenocarcinoma. *Nature* **545**, 355–359 (2017).

60. Yan, K. S. et al. Non-equivalence of Wnt and R-spondin ligands during Lgr5(+) intestinal stem-cell self-renewal. *Nature* **545**, 238–242 (2017).

61. Janda, C. Y. et al. Surrogate Wnt agonists that phenocopy canonical Wnt and beta-catenin signalling. *Nature* **545**, 234–237 (2017).

62. Ruan, K., Bao, S. & Ouyang, G. The multifaceted role of periostin in tumorigenesis. *Cell. Mol. Life Sci.* **66**, 2219–2230 (2009).

63. Wu, X. et al. TGM3, a candidate tumor suppressor gene, contributes to human head and neck cancer. *Mol. Cancer* **12**, 151 (2013).

64. Yeo, W. et al. Phase I/II study of temsirolimus for patients with unresectable hepatocellular carcinoma (HCC)—a correlative study to explore potential biomarkers for response. *BMC Cancer* **15**, 395 (2015).

65. Budwit-Novotny, D. A. et al. Immunohistochemical analysis of estrogen receptor in endometrial adenocarcinoma using a monoclonal antibody. *Cancer Res.* **46**, 5419–5425 (1986).

66. Azim, H. A. Jr et al. RANK-ligand (RANKL) expression in young breast cancer patients and during pregnancy. *Breast Cancer Res.* **17**, (2015).